

On the rising and sinking of granular bubbles and droplets

Jens P. Metzger¹, Ruben M. Strässle¹, Louis Girardin²,
Nicholas A. Conzelmann¹ and Christoph R. Müller^{1,†}

¹Department of Mechanical and Process Engineering, ETH Zurich, 8092 Zurich, CH

²Department of Mechanical Engineering, University College of London,
London W1W 7TS, UK

(Received 19 October 2021; revised 20 June 2022; accepted 20 June 2022)

Recently, the existence of so-called granular bubbles and droplets has been demonstrated experimentally. Granular bubbles and droplets are clusters of particles that respectively rise and sink if submerged in an aerated and vibrated bed of another granular material of different size and/or density. However, currently, there is no model that explains the coherent motion of these clusters and predicts the transition between a rising and sinking motion. Here, we propose an analytical model predicting accurately the neutral buoyancy limit of a granular bubble/droplet. This model allows the compilation of a regime map identifying five distinct regimes of granular bubble/droplet motion.

Key words: fluidized beds

1. Introduction

Granular materials are complex systems that can exhibit liquid-like behaviour under agitation. Examples are gas bubbles in gas–solid-fluidized beds (Davidson, Harrison & Carvalho 1977), breaking waves in granular shear layers (Goldfarb, Glasser & Shinbrot 2002), gas–solid fingering patterns akin to Rayleigh–Taylor instabilities (Vinningland *et al.* 2007) and condensation-like droplet formation of particles on tapped plates (Duran 2001). Very recently, McLaren *et al.* (2019) have observed further liquid-like phenomena in binary granular materials that are subjected to simultaneous vibration and aeration. When a cluster composed of particles with diameter d_c and density ρ_c is immersed in a bed of particles of different diameter d_b and density ρ_b , the cluster forms a coherent structure rising similar to a gas bubble in a liquid. Such clusters have been termed ‘granular bubbles’

† Email address for correspondence: muelchri@ethz.ch

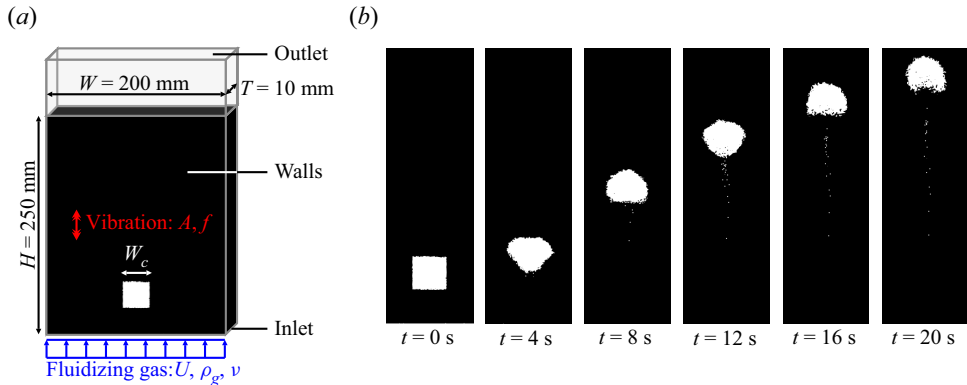


Figure 1. (a) Numerical set-up: bulk particles (black, $d_b = 1.16$ mm and $\rho_b = 6000$ kg m⁻³) are filled to a height H in a container of width W and depth T . Granular cluster particles (white) are initialized as a square cuboid ($W_c = 30$ mm) that is immersed in the bulk phase. The bed is subjected to a vertical, sinusoidal vibration ($A = 1$ mm and $f = 10$ Hz) and an upwards gas flow $U = 1.13$ m s⁻¹ with $\rho_g = 1.2$ kg m⁻³ and $\nu = 1.5 \times 10^{-5}$ m² s⁻¹. (b) Time series of a rising granular bubble formed by granular cluster particles ($d_c = 1.45$ mm and $\rho_c = 3000$ kg m⁻³). The images show a central cut out of the bed with a width of $0.375W$ and height H .

(see figure 1b) and have been observed to form for $d_c/d_b > 1$ and $\rho_c/\rho_b < 1$ albeit in the absence of surface tension at the cluster interface. Conversely, for $d_c/d_b < 1$ and $\rho_c/\rho_b > 1$ the cluster (termed a ‘granular droplet’) sinks and splits similar to a droplet of dense liquid falling in a miscible but lighter liquid. Despite some similarities with their fluid analogues, the mechanism driving granular bubbles and droplets must differ appreciably from their liquid counterparts as granular materials readily solidify under pressure and lose their fluidity due to frictional forces. McLaren *et al.* (2019) have argued that a granular bubble rises for $d_c > d_b$ as gas required to fluidize the granular material is drawn into the bubble, counteracting gravity through an increased drag. On the other hand, a granular droplet sinks for $d_c < d_b$ as gas bypasses the droplet. As the work of McLaren *et al.* (2019) was largely experimental, relying on only two different ratios for d_c/d_b and ρ_c/ρ_b , there is still very little understanding of the underlying physics of these new phenomena. Here, we derive an analytical model that predicts the neutral buoyancy limit of a granular cluster allowing the construction of a regime map. This regime map reveals the existence of three additional, previously unreported, regimes.

2. Numerical set-up

A critical assessment of the hypothesis of McLaren *et al.* (2019) concerning the transition between rising and sinking granular clusters requires quantitative information on the gas flow near a cluster. However, this information is not easily accessible by experiments due to the opaque nature of granular matter. To this end, computational fluid dynamics coupled to a discrete element method (CFD-DEM) was applied to simulate a pseudo-two-dimensional vibro-gas-fluidized bed using *cfDEMcoupling*[®] (Kloss *et al.* 2012). Details on the CFD-DEM model and the implemented equations can be found in Appendix A.

The gas flow field was calculated in cubic volume elements of 5 mm edge length using the built-in finite volume method solver of *cfDEMcoupling*[®] (Kloss *et al.* 2012). The boundary conditions used in the CFD are summarized in table 1. Due to the coarse resolution of the CFD mesh, a full-slip boundary condition was implemented between solid walls and the gas phase (Beetstra, van der Hoef & Kuipers 2007; Li *et al.* 2012;

Quantity		Inlet	Boundary Outlet	Walls
Reduced pressure	p/ρ_g	zero gradient	$10^5 \text{ m}^2 \text{ s}^{-2}$	zero gradient
Gas velocity	\mathbf{u}	$(0, U, 0)^T$	zero gradient	full slip

Table 1. Boundary conditions used in the CFD part.

Li, Zhang & Hernández-Jiménez 2016). However, the frictional and collisional contacts between the particles and the walls are fully resolved in the DEM. Studies of Zenit, Hunt & Brennen (1997) and Berzi & Fraccarollo (2015) have shown that particle collisions in inertia-dominated suspensions cause velocity and pressure fluctuations in the interstitial fluid that affect in turn the prevailing stresses and the effective viscosity of the fluid. In our work, the occurring fluid velocity fluctuations due to particle collisions are expected to be of the order of the magnitude of the peak particle velocities (that are $\sim 0.1 \text{ m s}^{-1}$), however, the interstitial gas velocity is approximately 30 times faster on average. Thus, we expect the drag force to dominate over local fluid forces due the collision-induced velocity fluctuations. As the local void fraction ϵ is fairly constant throughout the entire particle packing, viscous stresses from local flow compressibility are expected to be small and only shear stresses for the fluid stress tensor were used in (A4). Moreover, in our simulations, the fluid density ρ_g is low compared with the solid density of the particles. Thus, further fluid–particle interaction forces such as the added mass effect are minor and have been neglected (Sommerfeld 2018).

The numerical set-up of the vibro-gas-fluidized bed resembled the experiments of McLaren *et al.* (2019), see figure 1(a). Specifically, a box of width $W = 200 \text{ mm}$ and thickness $T = 10 \text{ mm}$ was filled up to a height of $H = 250 \text{ mm}$ with a polydisperse mixture of spherical particles, referred to as the bulk phase. The bulk particles had a density $\rho_b = 6000 \text{ kg m}^{-3}$ and a mean diameter $d_b = 1.16 \text{ mm}$. Polydispersity was introduced to reduce crystallization effects of the packing (Pusey 1987). To this end, 60 mass-% of the bulk particles had the nominal diameter d_b and 20 mass-% were attributed each to a particle size equal to $0.9d_b$ and $1.1d_b$, respectively. Inside the bulk phase, a square cuboid of width $W_c = 30 \text{ mm}$ and depth T was cut out and filled with spherical particles of mean diameter d_c and density ρ_c (referred to as the granular cluster). The cluster particles followed the same polydispersity scheme as the bulk particles. The lower edge of the cluster was 30 mm above the bottom of the bed. Details on the DEM particle properties are found in table 2.

In the present study, we reduced the coefficient of restitution e of the particles to 0.3 in order to speed up the simulations. However, a parameter study varying e showed that a variation of e in the range 0.1–0.95 has no significant influence on the evolution of granular bubbles, see Appendix E. At the bottom of the bed, an upwards gas flow with a superficial velocity $U = 1.13 \text{ m s}^{-1}$, density $\rho_g = 1.2 \text{ kg m}^{-3}$ and viscosity $\nu = 1.5 \times 10^{-5} \text{ m}^2 \text{ s}^{-1}$ entered the bed. The value of U was equal to the minimum fluidization velocity of the bulk particles ($U_{mf,b}$), i.e. the velocity at which the drag force balances the weight of the bulk particles in the gravitational field $g = 9.81 \text{ m s}^{-2}$ (Kunii & Levenspiel 1991). Fluidization reduced frictional forces between the bulk particles, a key requirement for granular clusters being able to rise/sink. During the simulations, the box was subjected to a vertical, sinusoidal vibration with an amplitude $A = 1 \text{ mm}$ and frequency $f = 10 \text{ Hz}$. Applying vibration aids the creation of a mobilized state of the granular material and reduces the

Quantity	Bulk particles	Cluster particles
Particle shape	Sphere	Sphere
Mean particle size	$d_b = 1.16 \text{ mm}$	$d_c = 0.5 \dots 3 \times d_b$
Particle size distribution (mass fraction)	$\Delta Q_3(d_b) = 0.6$ $\Delta Q_3(0.9d_b) = 0.2$ $\Delta Q_3(1.1d_b) = 0.2$	$\Delta Q_3(d_c) = 0.6$ $\Delta Q_3(0.9d_c) = 0.2$ $\Delta Q_3(1.1d_c) = 0.2$
Particle density	$\rho_b = 6000 \text{ kg m}^{-3}$	$\rho_c = 0.2 \dots 2 \times \rho_b$
Young's modulus	$E_b = 5 \text{ MPa}$	$E_c = 5 \text{ MPa}$
Poisson ratio	$\nu_b = 0.45$	$\nu_c = 0.45$
Coefficient of restitution	$e_b = 0.3$	$e_c = 0.3$
Coefficient of friction	$\mu_b = 0.15$	$\mu_c = 0.15$
Contact law	Hertzian	Hertzian

Table 2. Particle properties used in the DEM part.

emergence of gas bubbles that otherwise would arise if the particles were fluidized by gas alone (McLaren *et al.* 2019, 2021). This allowed the evolution of the granular clusters to be unimpaired by the presence and motion of large gas bubbles. Importantly, applying only vibration without gas fluidization did not establish any convective flow patterns in the bulk phase and lead to an immobile granular cluster.

3. Experimental set-up

In an effort to validate the regimes found in numerical simulations, additional experiments were performed matching the numerical set-up. To this end, a series of granular clusters was prepared in a pseudo-two-dimensional vibro-gas-fluidized bed made of acrylic glass sheets. The inner dimensions of the bed were $W = 200 \text{ mm}$ and $T = 10 \text{ mm}$. Analogue to the procedure described in Metzger *et al.* (2022), a granular cluster with $W_c = 30 \text{ mm}$ was initialized in a bed of bulk particles, ensuring a configuration as shown in figure 1(a). The height of the granular bed was set to $H = 250 \text{ mm}$. Table 3 lists all combinations of bulk and cluster particles that have been used in the experiments. During the experiments, a shaker (Labworks Inc., ET-139) vertically vibrated the fluidized bed at identical conditions used in the simulations, i.e. $A = 1 \text{ mm}$, $f = 10 \text{ Hz}$ and $\Gamma = 0.4$. A flow of pressurized air was used to fluidize the granular material at incipient fluidization conditions, i.e. $U/U_{mf,b} = 1$. The gas flow was controlled by a mass flow controller (Bronkhorst AG, F-202AV) and passed through a humidifier before entering the fluidized bed. Humidification of the fluidizing gas mitigated the build-up of electrostatic charges on the granular material. Additionally, the bulk materials were treated with anti-static spray (Electrolube, ASA250). Neither humidification nor anti-static coating led to the formation of liquid bridges such that the granular material maintained its free-flowing properties. The emergence of a granular cluster was recorded with a digital camera (Canon, EOS 77D) at a frame rate of 50 Hz. Each experiment listed in table 3 was repeated three times.

4. Derivation of the analytic gas shift model

First, we evaluate numerically the effect of a granular cluster on the gas flow field. Figures 2(a) and 2(b) display the gas flow in the vicinity and inside a granular cluster for two values of the relative particle diameter

$$d^* = d_c/d_b. \tag{4.1}$$

ID	d_b/mm	$\rho_b/(\text{kg m}^{-3})$	d_c/mm	$\rho_c/(\text{kg m}^{-3})$	d^*	$\Delta\rho^*$	Re_b	Regime
A	1.1 ± 0.1	6050	2.2 ± 0.2	2500	2	0.41	73.3	rising bubble
B	1.1 ± 0.1	6050	2.45 ± 0.15	5300	2.23	0.88	73.3	rising finger
C	1.1 ± 0.1	6050	2.35 ± 0.15	6130	2.14	1.01	73.3	rising finger
D	1.1 ± 0.1	6050	0.5 ± 0.1	9200	0.46	1.52	70.9	sinking droplet
E	1.5 ± 0.1	5300	2.45 ± 0.15	5300	1.63	1	103.3	rising finger
F	1.5 ± 0.1	5300	2.35 ± 0.15	6130	1.57	1.16	103.3	stagnant cone
G	1.5 ± 0.1	4100	2.7 ± 0.2	3700	1.8	0.90	91.7	rising finger
H	1.6 ± 0.1	3700	0.6 ± 0.1	4100	0.38	1.11	106.7	disintegrating bubble
I	1.45 ± 0.2	2500	2.35 ± 0.15	4100	1.62	1.64	64.5	sinking droplet
J	1.45 ± 0.2	2500	1.05 ± 0.05	6050	0.72	2.42	64.5	sinking droplet
K	1.45 ± 0.2	2500	2.35 ± 0.15	6130	1.62	2.45	64.5	sinking droplet

Table 3. Combination of bulk particles (index b) and cluster particles (index c) used in the experiments. All experiments were performed with vertical vibration ($A = 1 \text{ mm}$, $f = 10 \text{ Hz}$, $\Gamma = 0.4$) and at incipient fluidization ($U/U_{mf,b} = 1$). The particles were sieved and the \pm sign indicates the upper and lower bounds of the particle size. The values of $d^* = d_c/d_b$, $\Delta\rho^* = (\rho_c - \rho_g)(\rho_b - \rho_g)^{-1}$ and $Re_b = Ud_b/\nu$ were calculated based on the mean particle diameters and the nominal solid densities.

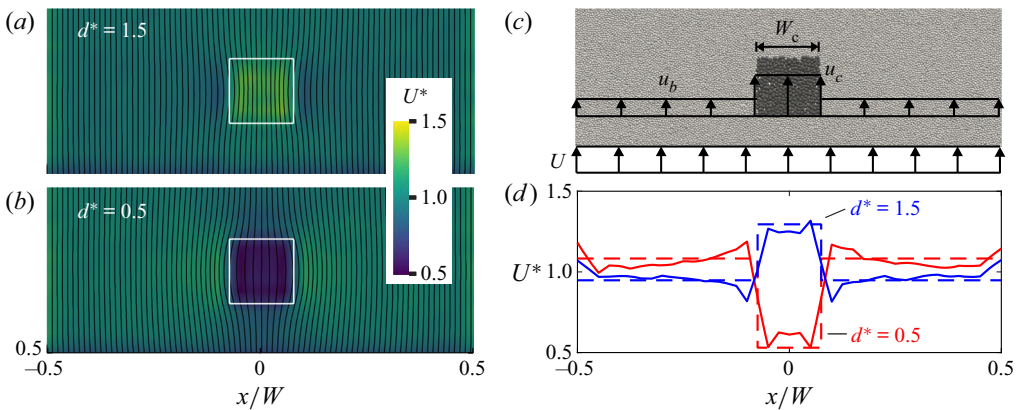


Figure 2. Heterogeneous gas flow near a square-shaped granular cluster of width $W_c = 30 \text{ mm}$. (a,b) Simulated gas flow with $Re_b = Ud_b/\nu = 88.75$ through a packing with $d^* = 1.5$ and 0.5 , respectively. The white boxes mark the edge of the granular cluster and the black curves show the gas streamlines. Here, U^* is given by the background colour. (c) Decomposition of U into u_c (cluster) and u_b (bulk phase) according to (4.2) and (4.4). (d) The value of U^* along the horizontal line through the centre of a granular cluster with, respectively, $d^* = 1.5$ (blue) and $d^* = 0.5$ (red). Solid lines plot the Eulerian-Lagrangian simulation results; dashed lines plot the solutions of the analytical model.

The black curves represent the gas streamlines and the background shows the dimensionless magnitude of the gas velocity $U^* = u/U$, where u is the magnitude of the local superficial gas velocity. For $d^* = 1.5$, the streamlines concentrate inside the granular bubble and U^* is higher in the cluster than in the surrounding bulk phase, i.e. gas flows preferentially through the granular cluster. For $d^* = 0.5$ the situation inverts. Such flow characteristics have been expected by Gilbertson & Eames (2001) and McLaren *et al.* (2019) due to an increased/reduced permeability with increasing/reduced particle size (Kozeny 1927; Carman 1937; Ergun 1952). The flow heterogeneity that is caused by the redirection of gas into or around a granular cluster will be referred to as ‘gas shift’ in

the following. This gas shift is key to explaining the rising and sinking of granular bubbles and droplets and hence has to be incorporated in any predictive analytical model.

In order to quantify the gas shift, we derive an analytical model for the gas flow around the granular cluster. For the model we apply a horizontal cut through the centre of the granular cluster that divides the bed into two regions: the cluster of dimensionless width $W^* = W_c/W$ and the bulk phase of dimensionless width $(1 - W^*)$, as shown in [figure 2\(c\)](#). The gas that enters the bed is decomposed into two parallel flows through these two regions. Gas is assumed to flow with a uniform dimensionless velocity $U_c^* = u_c/U$ and $U_b^* = u_b/U$ through the cluster and bulk phase, respectively. Due to its low velocity, the gas flow is assumed to be incompressible and the continuity equation reads

$$1 = (1 - W^*)U_b^* + W^*U_c^*. \tag{4.2}$$

[Figures 2\(a\)](#) and [2\(b\)](#) show parallel and equally spaced streamlines below and above the granular cluster, i.e. no horizontal pressure gradients exist in these regions. This implies that the gas flow through the cluster is driven by the same vertical pressure drop as the flow through the adjacent bulk phase. Ergun’s equation ([Ergun 1952](#)) is used to quantify the pressure drop Δp across a height L of cluster or bulk phase particles

$$\frac{\Delta p_i}{L} = \frac{150\mu_g}{d_i^2} \frac{(1 - \epsilon_i)^2}{\epsilon_i^3} u_i + \frac{1.75\rho_g}{d_i} \frac{1 - \epsilon_i}{\epsilon_i^3} u_i^2, \tag{4.3}$$

where index $i = [b, c]$ denotes the bulk or cluster phase, respectively, and $\mu_g = \nu\rho_g$ is the dynamic gas viscosity. Equating $\Delta p_c/L = \Delta p_b/L$ and rewriting the equation in a non-dimensional form yields a correlation between U_b^* , U_c^* , d^* , the void fraction ϵ and the Reynolds number of the bulk phase $Re_b = Ud_b/\nu$, see [Appendix B](#) for the full derivation. According to our computational simulations, ϵ is very uniform in the bed ($\epsilon \approx 0.4$) for a large range of d_c and d_b provided that the coefficients of friction of the bulk and cluster particles are identical. Given these boundary conditions, we obtain

$$0 = \left(U_b^* - \frac{U_c^*}{d^{*2}} \right) + \frac{Re_b}{k} \left(U_b^{*2} - \frac{U_c^{*2}}{d^*} \right), \tag{4.4}$$

with $k = 85.7(1 - \epsilon) \approx 51.42$. When μ_b and μ_c differ substantially, the assumption of a uniform void fraction ϵ is no longer satisfied. This case is described in [Appendix D](#). In the following, only cases with identical coefficients of friction are considered. Combining [\(4.2\)](#) and [\(4.4\)](#) allows us to determine U_c^* and U_b^* as a function of Re_b , d^* and W^* . [Figure 2\(d\)](#) compares the values of U^* along a horizontal line through the centre of a cluster obtained by the Eulerian–Lagrangian simulation (solid lines) with the analytical model (dashed lines). For both values of d^* , the analytical model gives an accurate quantitative prediction of the average gas velocity inside the granular cluster and the bulk phase, although not all local effects (e.g. wall effects at $|x/W| = 0.5$ or local depletion/accumulation of gas flow in the bulk phase for $0.075 \leq |x/W| \leq 0.16$ due to the gas shift) are captured in the analytical model. Based on this finding, U_c^* can be used as a quantitative measure for the gas shift as $U_c^* > 1$ indicates an increased gas flow inside the granular cluster compared with the inlet gas velocity U . Inversely, $U_c^* < 1$ denotes a reduced gas flow in the cluster. A further evidence for the validity of the analytical gas shift model is presented in [figure 3\(a\)](#) plotting U_c^* vs d^* . Here, the predictions of the gas shift model agree very well with the results of the Eulerian–Lagrangian simulations ($W^* = 0.15$). The analytical model further indicates that U_c^* depends on the dimensionless width of the cluster W^* . An increase in W^* yields higher values of U_c^* for $d^* < 1$ and lower

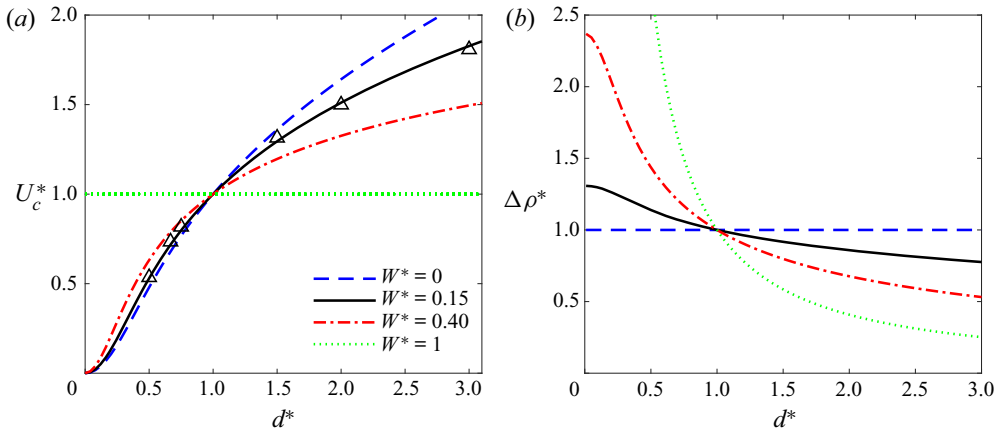


Figure 3. (a) Gas shift (U_c^*) occurring in granular clusters of particle size d^* as predicted by (4.2) and (4.4) for a series of widths W^* . Triangles (Δ) represent the results of the Eulerian-Lagrangian simulations for U_c^* with $W^* = 0.15$. (b) Neutral buoyancy limits predicted for granular clusters of varying W^* (4.2), (4.4) and (5.2) with $\Delta\rho^* = (\rho_c - \rho_g)(\rho_b - \rho_g)^{-1}$. Both panels (a,b) use $Re_b = 88.75$ and $Ar_b = 3.40 \times 10^5$.

values for $d^* > 1$. This is because, for a fixed W , an increasing width of the granular cluster reduces the size of the bulk phase from which gas is withdrawn ($d^* > 1$) or into which additional gas is shifted ($d^* < 1$); thus, $U_c^* \rightarrow 1$ for $W^* \rightarrow 1$. Inversely, U_c^* approaches a finite value for $W^* \rightarrow 0$. This solution represents the maximal obtainable gas shift to/from an infinitely small cluster for a given d^* and Re_b .

5. Derivation of the neutral buoyancy limit

As the analytical model is able to accurately predict the gas shift to/from the granular cluster to the bulk phase, we address next the question of under which circumstances a granular cluster rises or sinks. In our model we use two assumptions: first, the inlet gas velocity U is set to the minimum fluidization velocity of the bulk particles $U_{mf,b}$, i.e. the velocity of the gas flow required to induce a drag force that equals the weight of the particles. Here, $U_{mf,i}$ is determined from a force balance equating the pressure drop across the packing (4.3) with the weight of the packing per cross-sectional area such that

$$\frac{\Delta p_i}{L} = \frac{150\rho_g v}{d_i^2} \frac{(1-\epsilon)^2}{\epsilon^3} U_{mf,i} + \frac{1.75\rho_g}{d_i} \frac{1-\epsilon}{\epsilon^3} U_{mf,i}^2 = (1-\epsilon)(\rho_i - \rho_g)g, \quad (5.1)$$

where $i = [b, c]$ (Kunii & Levenspiel 1991). Rearranging the right-hand sides and introducing the Reynolds number $Re_{mf,i} = d_i U_{mf,i} v^{-1}$ and the Archimedes number $Ar_i = d_i^3 (\rho_i - \rho_g) (\rho_g v^2)^{-1}$ yields

$$\frac{1.75}{\epsilon^3} Re_{mf,i}^2 + \frac{150(1-\epsilon)}{\epsilon^3} Re_{mf,i} = Ar_i. \quad (5.2)$$

Thus, for constant ϵ and v , $Re_{mf,b}$ and $U_{mf,b}$ are only functions of Ar_b and d_b . Applying this assumption to the bulk particles ($\rho_b = 6000 \text{ kg m}^{-3}$, $d_b = 1.16 \text{ mm}$, $\epsilon = 0.4$) and air ($\rho_g = 1.2 \text{ kg m}^{-3}$, $v = 1.5 \times 10^{-5} \text{ m}^2 \text{ s}^{-1}$) yields $U = U_{mf,b} = 1.13 \text{ m s}^{-1}$.

Secondly, we assume that the rising/sinking of a cluster is driven by the degree of fluidization of the cluster particles due to the gas flow. This assumption is based on findings by Liu *et al.* (2010) and Li *et al.* (2017a,b, 2019) who have studied size

separation in binary granular materials that have been subjected to combined vibration and fluidizing gas flow. Their research revealed a competition between vibration-induced size separation as well known from the Brazil nut effect (Rosato *et al.* 1987; Knight, Jaeger & Nagel 1993; Huerta & Ruiz-Suárez 2004) and its reverse (Hong, Quinn & Luding 2001; Jenkins & Yoon 2002; Trujillo, Alam & Herrmann 2003; Breu *et al.* 2003; Shinbrot 2004; Alam, Trujillo & Herrmann 2006) and gas-flow-induced size separation due to differences between the drag and gravitational forces acting on the particles. They found that if the gas velocity U is close to or above the minimum fluidization velocity of a granular material, size separation can be governed by gas flow effects even for strong vibrational accelerations $\Gamma = A(2\pi f)^2/g > 1$. Under such boundary conditions, binary granular materials segregate according to their U_{mf} values with the material of lower U_{mf} segregating on top of the material with the higher U_{mf} . In our studies, we use $\Gamma = 0.4$ and $U = U_{mf,b}$, i.e. size separation is dominated by gas flow effects. Hence, we hypothesize that a granular bubble rises if the gas flow through the granular bubble gives rise to a drag force that is larger than the particle weight ($u_c > U_{mf,c}$) and the granular droplet sinks for $u_c < U_{mf,c}$; a granular cluster is neutrally buoyant if $u_c = U_{mf,c}$. From the analytical gas shift model we have $u_c = UU_c^*$ and $U_{mf,c}$ can be calculated via (5.2). Although vibration may reduce U_{mf} of granular particles for $\Gamma \geq 1$ (Gupta & Mujumdar 1980; Mawatari, Tatemoto & Noda 2003) and $\Gamma < 1$ (McLaren *et al.* 2021), we assumed that vibration does not affect appreciably the neutral buoyancy limit of the granular cluster because the net drag that leads to the rise of a granular bubble is dominated by the effective gas flow. Small fluctuations in the drag force due to vibration are expected to cancel out over a full vibration cycle. However, the dynamics of a granular material in a vibro-gas-fluidized bed might change once the vibrational acceleration exceeds gravity, i.e. for $\Gamma > 1$. Hence, to restrict the potential influence of vibration on the emergence of a granular cluster and ensure validity of the previous assumptions, we limit the following derivation to $\Gamma < 1$.

With these two assumptions at hand, the neutral buoyancy limit can be calculated as a function of d^* , W^* , Re_b and Ar_b . Figure 3(b) plots the relative density difference

$$\Delta\rho^* = (\rho_c - \rho_g) (\rho_b - \rho_g)^{-1} \tag{5.3}$$

required to establish a neutrally buoyant granular cluster of width W^* as a function of d^* at constant U (later referred to as the ‘neutral buoyancy limit’). We observe that $\Delta\rho^*$ decreases monotonically with increasing d^* . For $d^* < 1$, the density of the cluster particles must be larger than the density of the bulk particles to achieve neutral buoyancy, and *vice versa* for $d^* > 1$. The monotonic behaviour is due to the particle size dependence of $U_{mf,c}$. This dependence is depicted for $W^* = 1$, i.e. the entire bed is filled with cluster particles and no gas shift occurs ($U_c^* = 1$). Here, a constant U leads to $\Delta\rho^* \rightarrow \infty$ (0) when $d^* \rightarrow 0$ (∞). For $W^* < 1$, the $\Delta\rho^*$ -curves increasingly flatten with decreasing W^* due to the gas shift to/from the granular cluster. As confirmed in Appendix C, the density of the cluster particles must be equal to the density of the bulk particles to be neutrally buoyant for $W^* \rightarrow 0$ (dashed line in figure 3b). To summarize, our model predicts a granular bubble to rise if $\Delta\rho^*$ is below the neutral buoyancy limit for any given Ar_b , Re_b , W^* and d^* , otherwise a granular droplet sinks.

6. Construction of a regime map

Using the present analytical model, we constructed a regime map that predicts the rising or sinking of a granular bubble/droplet of a given size W^* (figure 4). In order to test the validity of the regime map, numerical simulations were performed to probe the $\Delta\rho^*$ - d^* space for a fixed cluster size of $W^* = 0.15$, $Re_b = 88.75$ and $Ar_b = 3.40 \times 10^5$.

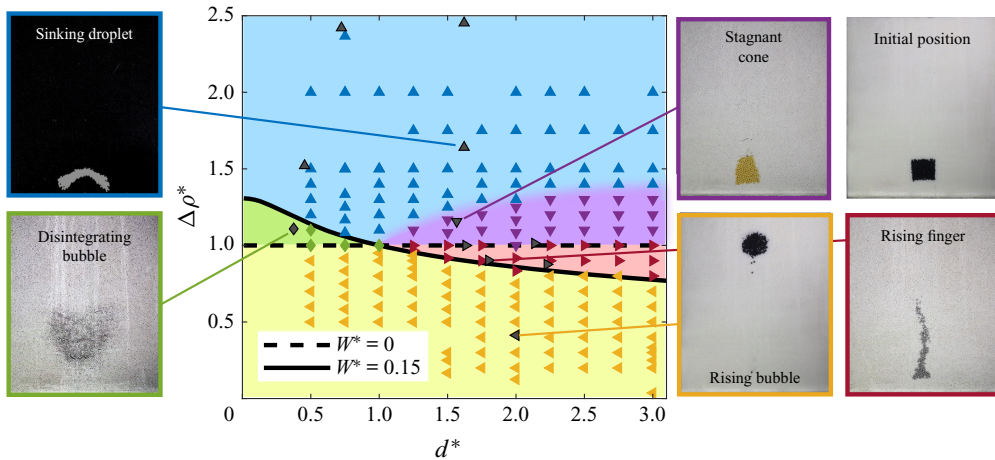


Figure 4. Regime map for a granular cluster with $W^* = 0.15$, $Re_b = 88.75$ and $Ar_b = 3.40 \times 10^5$. The solid and dashed lines are the neutral buoyancy limits for $W^* = 0.15$ and 0 , respectively. The following regimes are observed: sinking droplet (\blacktriangle , blue region), stagnant cone (∇ , purple region), rising finger (\blacktriangleright , red region), rising bubble (\blacktriangleleft , yellow region) and disintegrating bubble (\blacklozenge , green region). Coloured symbols are the results of the Eulerian–Lagrangian simulations. The grey filled symbols are results of the experiments listed in table 3. The images show a snapshot of the transformation of an initially square-shaped cluster in the respective regime.

Examples of such simulations are depicted in the time series shown in the figures 5, 8, 9, 10 and 11. The occurring motion patterns of the different granular clusters simulated were classified and marked in the regime map (figure 4). Five different regimes were identified: rising bubbles, rising fingers, disintegrating bubbles, sinking droplets and stagnant cones. The previous experimental study of McLaren *et al.* (2019) has identified only the rising bubble and sinking droplet regimes. As can be seen in the regime map, the first four regimes are in agreement with our neutral buoyancy model and their regime boundaries coincide with the neutral buoyancy limit for $W^* = 0.15$ and $W^* = 0$ (i.e. $\Delta\rho^* = 1$). Moreover, the experiments summarized in table 3 align with this regime map and agree with the numerical findings. As can be seen in figure 4, the existence of all five regimes can be confirmed by experiments. In the following, the characteristics of the different regimes will be discussed.

6.1. Rising bubble regime

Rising bubbles occur if $\Delta\rho^*$ is below the neutral buoyancy limit of the cluster for $d^* \geq 1$ or below $\Delta\rho^* = 1$ for $d^* < 1$ (\blacktriangleleft , yellow region in figure 4). In this region, the cluster particles form a bubble that rises through the bulk phase to the top of the bed, as seen in figure 5. Rising granular bubbles form when the gas velocity in the bubble exceeds the minimum fluidization velocity of the cluster particles and an effective drag pushes the cluster particles upwards.

As can be seen in figure 6(b), the cluster particles within a granular bubble exhibit a circulation flow that resembles vortex structures found in fluid bubbles rising in a denser fluid (Hill & Henrici 1894; Hadamard 1911; Rybczynski 1911; Batchelor 2000). Particles from the centre of the bubble move towards its roof, whereas particles close to the side boundaries of the bubble move towards its bottom. At the bubble wake, individual particles detach, forming a tail. The existence of such an internal circulation pattern in granular bubbles points to a fluid-like state of granular matter in and around

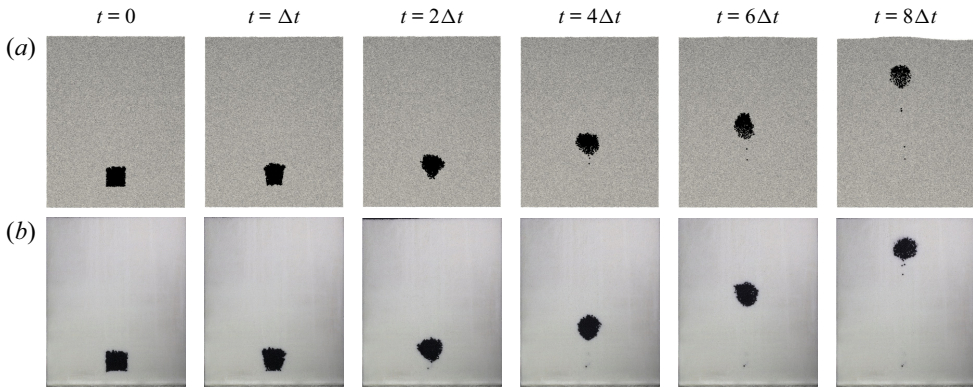


Figure 5. Time series of a rising bubble as obtained by (a) simulations and (b) experiments (table 3 A). Both rows show a cluster with $d^* = 2$ and $\Delta\rho^* = 0.9$. Time steps of the images are $\Delta t = 0.5$ s for simulations and 1 s for experiments.

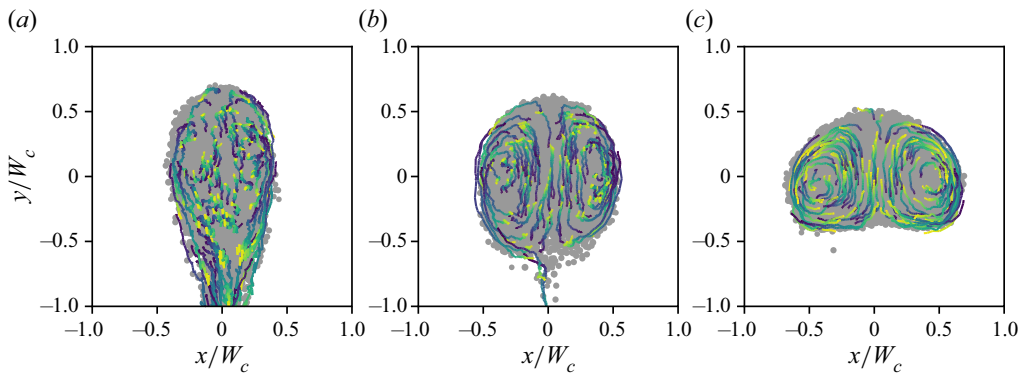


Figure 6. Motion of the cluster particles within a rising granular bubble for $\Delta\rho^* = 0.9$ (a), 0.8 (b) and 0.4 (c). Trajectories of 100 particles are shown in a reference frame moving with the centre of mass of the bubble. The colour grading of the trajectories corresponds to the progressing time with dark violet for a bubble at $t(y/H = 0.4)$ and bright yellow at $t(y/H = 0.8)$. The background shows the location of the cluster particles (grey) when the top of the bubble has reached the height $y/H = 0.8$ in the bed. All results were obtained from simulations with $W^* = 0.15$, $Re_b = 88.75$, $Ar_b = 3.40 \times 10^5$ and $d^* = 1.25$.

the bubble. A comparison of the panels of figure 6 reveals that the shape of the bubble and the circulation pattern therein depend on $\Delta\rho^*$. For small values of $\Delta\rho^*$ far away from the neutral buoyancy limit, e.g. $\Delta\rho^* = 0.4$ in (c), the bubble is spherical cap-shaped and exhibits a pronounced circulation flow. Increasing $\Delta\rho^*$ to 0.8 (figure 6b) yields a spherical bubble and a circulation pattern which has striking similarities to Hill's spherical vortex (Hill & Henrici 1894). Increasing $\Delta\rho^*$ further towards the neutral buoyancy limit leads to elongated bubbles with an attenuated inner circulation pattern and a pronounced tail, as can be seen in figure 6(a) and figure 7. This observation raises the question of why a tail is only formed for certain types of granular bubbles. To answer this, we have analysed the number of particles N_{Tail} that are found in the tail after a bubble has reached a height of $y/H = 0.8$ for various combinations of d^* and $\Delta\rho^*$. Following Nitsche & Batchelor (1997), who have studied the break-up of a falling drop containing suspended particles in a liquid, all particles within a vertical distance of $1.5W_c$ below the topmost cluster particle are considered to be in the bubble. All other particles are

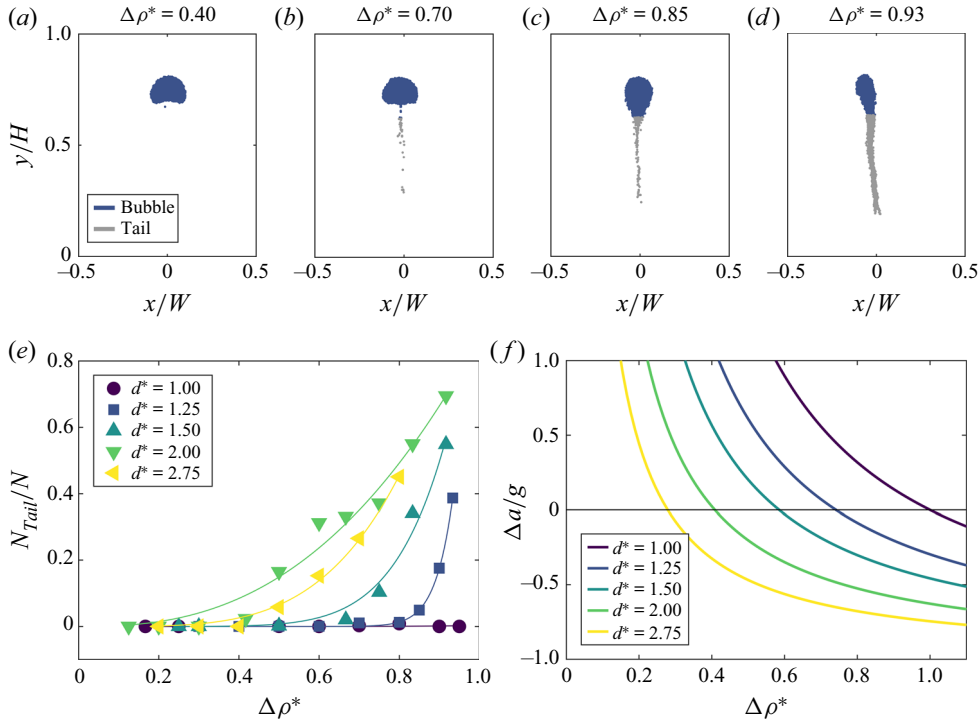


Figure 7. Emergence of a particle tail in the wake of a rising granular bubble. Panels (a–d) show granular bubbles as a function of $\Delta\rho^*$ with $d^* = 1.25$, when their roof has reached $y/H = 0.8$. In analogy to Nitsche & Batchelor (1997), all particles within a vertical distance of $1.5W_c$ from the topmost particle are considered to be part of the bubble (blue), otherwise the particles are considered to be part of the tail (grey). (e) The number of particles found in the tail N_{Tail} normalized by the number of particles initialized in the bubble N . The value of N_{Tail}/N depends on d^* and $\Delta\rho^*$. All points are obtained from numerical simulations of bubbles at $y/H = 0.8$. The lines are fitted power functions and only guidelines to the eyes. (f) Dependence of the normalized, effective drag of a cluster particle $\Delta a/g$ on $\Delta\rho^*$ for varying d^* . $\Delta a/g = (|\mathbf{F}_{d,c}| - mg)/(mg) = 1 - (U/U_{mf,c})^2$ for constant ϵ and $U \geq U_{mf,c}$ with $U_{mf,c}$ calculated from (5.2).

regarded as part of the tail. Figure 7(a–d) shows the division of cluster particles into bubble and tail particles for granular bubbles using $d^* = 1.25$ and $\Delta\rho^* = 0.4, 0.7, 0.85$, and 0.93 , respectively. Again, the size of the tail increases for increasing $\Delta\rho^*$. Figure 7(e) displays the ratio of N_{Tail} to the total number of cluster particles N as a function of d^* and $\Delta\rho^*$. It can be seen that, for $d^* > 1$, N_{Tail}/N is close to zero for small values of $\Delta\rho^*$. Once $\Delta\rho^*$ exceeds a certain threshold, the number of particles in the tail increases significantly with increasing cluster particle density. This threshold decreases monotonically from 0.8 for $d^* = 1.25$ to 0.4 for $d^* = 2$. Only for $d^* = 2.75$ the threshold seems to be increasing again. For clusters with $d^* \leq 1$ no significant tail is formed at all and N_{Tail}/N is (close to) zero. A possible explanation for the onset of tailing can be found when inspecting the effective drag acting on the cluster particles. According to Li *et al.* (2017a), the effective acceleration on a particle in a vibro-gas-fluidized system can be expressed as $\Delta a/g = (|\mathbf{F}_{d,c}| - mg)/(mg) = 1 - (U/U_{mf,c})^2$ provided ϵ is constant and drag dominates vibration in particle segregation. Imagine a single particle detaches from a granular bubble, leaves the zone of preferential gas flow and disperses in the bulk phase. This particle is only able to rise if the drag on it exceeds gravity, i.e. $\Delta a/g > 0$, otherwise

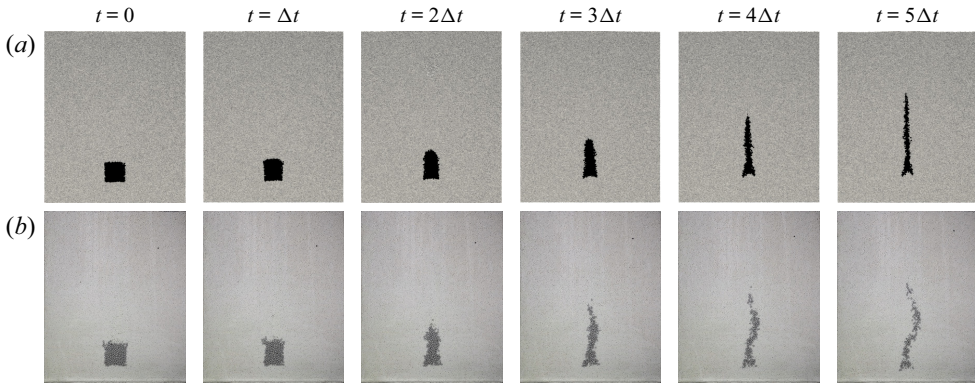


Figure 8. Time series of a rising finger. (a) Euler–Lagrange simulation of a cluster with $d^* = 1.75$, $\Delta\rho^* = 0.9$ and $\Delta t = 2$ s. (b) Experiment (table 3 G) with $d^* = 1.8$, $\Delta\rho^* = 0.9$ and $\Delta t = 8$ s.

it would stay in the tail. Hence the particle would rise if the local superficial gas velocity u exceeds the minimum fluidization velocity $U_{mf,c}$. Since the detached cluster particle is surrounded by bulk particles only, u will be close to the inlet velocity of the fluidized bed U . Using this information, one can readily plot the effective drag for various diameters d^* (figure 7*f*). Indeed, the roots of $\Delta a/g = 0$ (for a given d^*) predict well the thresholds for tailing found in figure 7(*e*). However, simulations with $d^* = 2.75$ fall outside this trend. This could be explained by the fact that the cluster particles are fairly large compared with the bulk particles and distort the local packing structure changing in turn the gas flow field. Despite the similarities of a granular bubble with sedimenting particle droplets (Nitsche & Batchelor 1997), a mathematical relation for the rate of particles leaving the bubble has not yet been found.

6.2. Rising finger regime

The strong tailing of a granular cluster as $\Delta\rho^*$ approaches the neutral buoyancy limit leads to a change in the motion behaviour of the cluster. Instead of rising as a coherent, spherical collective, the cluster forms an elongated and thinning stream of particles rising in the bulk phase. This change in the motion dynamics indicates the existence of a distinct regime, here referred to as rising fingers. Rising fingers occur for clusters with $d^* > 1$ and $\Delta\rho^*$ between the neutral buoyancy limit and $\Delta\rho^* = 1$ (\triangleright , red region in figure 4). An example for a rising finger is given in figure 8. The finger is thickest for $\Delta\rho^*$ close to the neutral buoyancy limit ($W^* = 0.15$) and becomes thinner as $\Delta\rho^*$ approaches unity. The motion of a granular finger is described in two stages: at first, the rising finger elongates quickly, where the lower part of the finger is almost stagnant and only the top part is moving upwards. As the finger becomes thinner, the rise speed of the top part of the finger decays until it almost stops rising. Rising granular fingers seldom reach the top surface of the fluidized bed. Analysis of the gas flow within a rising finger reveals that the initial elongation of a rising finger is driven by an increased gas flow inside the granular finger. After a strong elongation and thinning of the finger, the cluster particles are then propelled by small gas bubbles that form in the top part of the finger. Our analytical model helps explain the emergence of rising fingers: if $\Delta\rho^*$ is larger than the neutral buoyancy limit, u_c is insufficient to levitate the entire granular cluster. However, decreasing the cluster width increases the gas velocity inside the finger (see figure 3*a*) such that the cluster particles experience a positive effective drag. Thus, the rising finger is stabilized by its

On the rising and sinking of granular bubbles and droplets

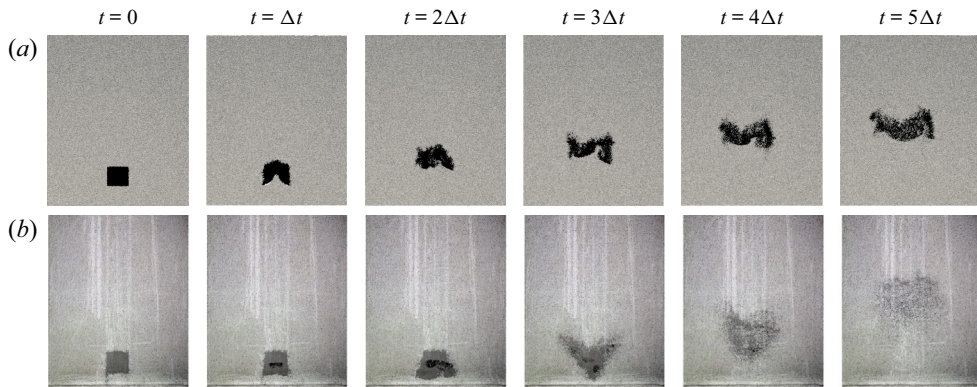


Figure 9. Time series of a disintegrating bubble. (a) Euler–Lagrange simulation of a cluster with $d^* = 0.5$, $\Delta\rho^* = 1.1$ and $\Delta t = 2.4$ s. (b) Experiment (table 3 H) with $d^* = 0.38$, $\Delta\rho^* = 1.11$ and $\Delta t = 6$ s. In the experiment, cluster particles are dark grey, bulk particles are light grey, whereas emerging gas bubbles are black.

decreasing thickness. During elongation, the width of the finger decreases until the cluster particles stop behaving as a coherent cluster due to their immersion into the bulk phase. As there is still an increased permeability of the packing due to the larger cluster particles, gas flows preferentially along this thin tail forming small gas bubbles at the top of the finger as u strongly exceeds $U_{mf,b}$ in this region.

6.3. Disintegrating bubble regime

In contrast to the self-stabilized rising fingers, disintegrating bubbles form for $d^* < 1$ and $\Delta\rho^*$ between unity and the neutral buoyancy limit (\diamond , green region in figure 4). Here, the cluster can rise as a coherent granular bubble, but particle fluctuations and emerging gas bubbles during its rise induce its disintegration as seen in figure 9. According to our model, the granular bubble particles rise because $\Delta\rho^*$ is below the neutral buoyancy limit. However, the low $U_{mf,c}$ of the cluster particles combined with the low permeability ($d^* < 1$) of the cluster makes this granular bubble an unstable configuration. In the case that a small void is created in the granular cluster due to the vibrations, gas suddenly flows into this highly permeable region of the cluster and increases the gas velocity. The gas flow inflates the size of the void and pushes the cluster particles upwards into the bulk phase. Repetitions of this process lead to a disintegrating bubble. If the cluster particles are sufficiently small compared with the bulk particles, they disperse in the surrounding bulk phase filling the interstitial voids, as seen in figure 9(b).

6.4. Sinking droplet regime

For values of $\Delta\rho^*$ significantly larger than unity, a granular droplet sinks (Δ , blue region in figure 4), as the cluster particles are too heavy to be carried up by the drag exerted by the gas flow. During its descent, the sinking droplet flattens and performs ultimately a binary split (figure 10). The splitting of such a granular droplet is not caused by the cluster's proximity to the bottom of the fluidized bed, but is a property that also exists for larger distances to the confining walls. McLaren *et al.* (2019) discovered the splitting of these droplets and a detailed analysis on the mechanism behind the droplet splitting can be found in Metzger *et al.* (2022).

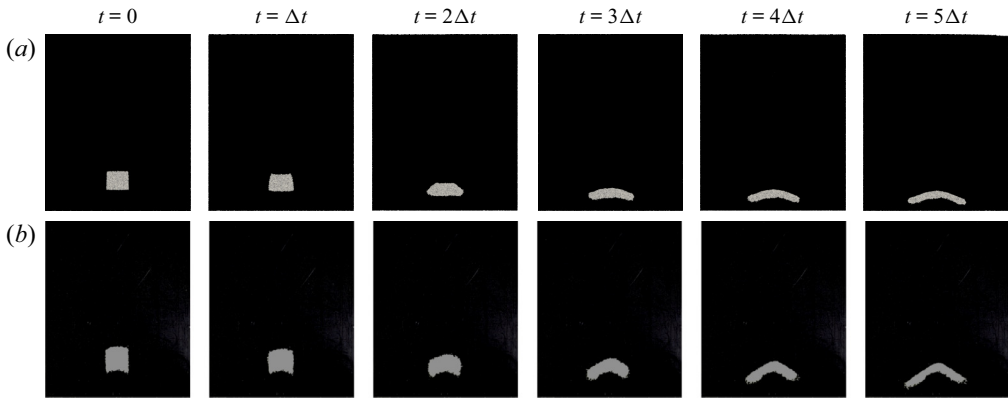


Figure 10. Time series of a sinking droplet. (a) Euler–Lagrange simulation of a cluster with $d^* = 0.75$, $\Delta\rho^* = 2.38$ and $\Delta t = 1$ s. (b) Experiment (table 3 J) with $d^* = 0.72$, $\Delta\rho^* = 2.42$ and $\Delta t = 2$ s.

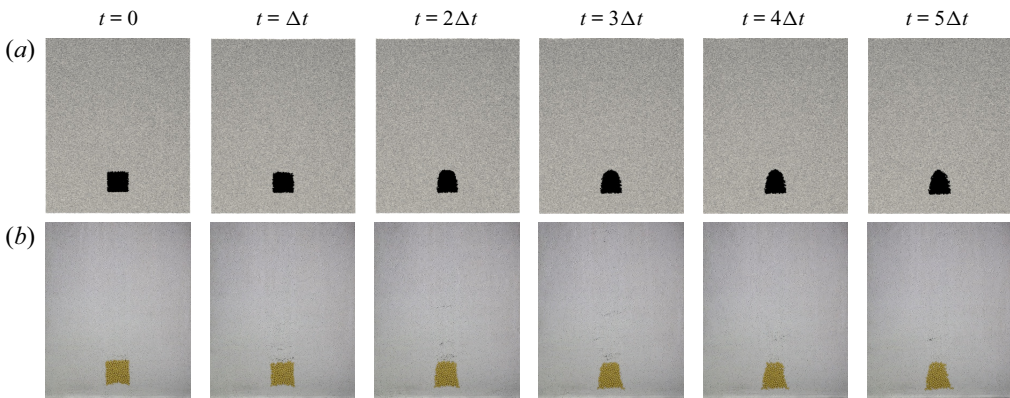


Figure 11. Time series of a stagnant cone. (a) Euler–Lagrange simulation of a cluster with $d^* = 1.75$, $\Delta\rho^* = 1.2$ and $\Delta t = 4$ s. (b) Experiment (table 3 F) with $d^* = 1.57$, $\Delta\rho^* = 1.16$ and $\Delta t = 60$ s.

6.5. Stagnant cone regime

Although the analytical model predicts that all droplets with $d^* > 1$ and $\Delta\rho^* > 1$ sink, there is a region for $\Delta\rho^* \geq 1$ and $d^* > 1$, where droplets become stagnant and develop a conical shape, termed the stagnant cone (∇ , purple region in figure 4). The lower limit of the stagnant cone regime is at $\Delta\rho^* = 1$ and the upper limit increases with increasing d^* . As the stagnant cone particles are too heavy to be neutrally buoyant ($\Delta\rho^* > 1$), the cluster acts as an additional load and inhibits fluidization of the bulk particles underneath the cluster. However, the net gravitational force of the cluster cannot overcome the interparticle friction in this unfluidized bulk region and thus the cluster remains stagnant. The formation of a cone (figure 11) can be explained by small fluctuations in the local gas velocity due to bed vibration. These fluctuations lead to a temporary fluidization of the cluster particles at the top of the cluster, such that they rearrange to an incipient granular finger. However, the fluctuations cannot maintain fluidization conditions for an extended duration of time, i.e. the cluster particles rest on top of the granular cluster. For $\Delta\rho^* \rightarrow 1$, the cone sharpens further until it finally merges into a rising finger for $\Delta\rho^* = 1$.

6.6. Further considerations

We have performed additional numerical Eulerian–Lagrangian simulations in which we varied the cluster width and were able to confirm the validity of the neutral buoyancy limit for a series of $W^* = [0.1, 0.15, 0.3, 0.4]$. However, the derivation of our model requires $d_c/W_c \ll 1$ to allow for enough particles in the granular cluster to justify the use of Ergun's equation (Ergun 1952). Also, our model is most accurate for $0.4 < d^* < 2.5$, as outside these limits small particles percolate into the interstitial voids of the larger particles and change the permeability of the cluster packing.

7. Conclusion




We have investigated the physics controlling the motion of a granular cluster in a pseudo-two-dimensional vibro-gas-fluidized bed. A granular cluster is an agglomeration of granular particles of certain size and density that is submersed in a bulk of particles with different particle size and/or density. When fluidized by combining vibration and gas flow, the granular cluster either rises coherently to the freeboard of the bed (granular bubble) or sinks to the bottom of the bed (granular droplet) depending on the relative size and relative density of the cluster particles and the bulk particles (McLaren *et al.* 2019). This work investigated the transition between rising granular bubbles and sinking granular droplets and identified the conditions required to form neutrally buoyant granular clusters. Eulerian–Lagrangian simulations revealed the existence of a gas flow heterogeneity in the proximity of a granular cluster, where gas flows preferentially through regions of larger particles due to their increased permeability. This shift in the gas flow pattern (into or out of the granular cluster) affects locally the degree of fluidization of the particles in and around the cluster and in turn significantly influences the motion of the granular cluster itself. Based on a dimensionless gas shift model, we proposed an analytical model predicting the neutral buoyancy limit of a granular cluster assuming that under this condition the local gas velocity matches the minimum fluidization velocity $U_{mf,c}$ of the cluster particles. If the gas velocity is higher or lower than $U_{mf,c}$, the cluster rises or sinks, respectively. Finally, a dimensionless regime map was compiled and tested against both extensive Eulerian–Lagrangian simulations and experiments. This regime map correctly predicts the regimes of rising bubbles and sinking droplets and revealed three distinct, previously unreported, regimes in the transition region: rising fingers, disintegrating bubbles and stagnant cones.

Funding. This work was supported by the Swiss National Science Foundation (grant number 200020_182692).

Declaration of interests. The authors report no conflict of interest.

Data availability statement. The data that support the findings of this study are available from the corresponding author upon request. This publication was created as part of NCCR Catalysis (grant number 180544), a National Centre of Competence in Research funded by the Swiss National Science Foundation.

Author ORCIDs.

-  Jens P. Metzger <https://orcid.org/0000-0002-1326-8204>;
-  Louis Girardin <https://orcid.org/0000-0002-8017-2405>;
-  Nicholas A. Conzelmann <https://orcid.org/0000-0002-5568-4863>;
-  Christoph R. Müller <https://orcid.org/0000-0003-2234-6902>.

Appendix A. Model equations implemented in the CFD-DEM

DEM was proposed initially by Cundall & Strack (1979) and uses a Lagrangian description of the particle phase. The trajectories of the individual particles are determined by the action of interparticle contact forces $F_{c,j}$, torques $M_{c,j}$, gravity \mathbf{g} and the drag force $F_{d,j}$ exerted by the fluid flow around the particles (Tsuji, Kawaguchi & Tanaka 1993; Zhou *et al.* 2010). Momentum equations for the translational and rotational motion were solved for each particle j of mass m_j and diameter d_j viz.

$$m_j \frac{d^2 \mathbf{x}_j}{dt^2} = \mathbf{F}_{c,j} + \mathbf{F}_{d,j} + m_j \mathbf{g}, \tag{A1}$$

$$\frac{1}{10} m_j d_j^2 \frac{d\boldsymbol{\omega}_j}{dt} = \mathbf{M}_{c,j}. \tag{A2}$$

Here, \mathbf{x}_j denotes the position and $\boldsymbol{\omega}_j$ the angular velocity of the particle. Details on the implemented contact laws for $\mathbf{F}_{c,j}$ and $\mathbf{M}_{c,j}$ are described by Kloss *et al.* (2012). The gas flow (CFD, Eulerian description) was modelled by an incompressible, two-phase formulation of the Navier–Stokes equations including a term \mathbf{R} to capture the momentum exchange between the gas phase and the suspended particles (Zhou *et al.* 2010)

$$\frac{\partial \epsilon}{\partial t} + \nabla \cdot (\epsilon \mathbf{u}) = 0, \tag{A3}$$

$$\frac{\partial (\epsilon \mathbf{u})}{\partial t} + \nabla \cdot (\epsilon \mathbf{u} \mathbf{u}) = -\epsilon \frac{\nabla p}{\rho_g} - \frac{\mathbf{R}}{\rho_g} + \epsilon \nu \nabla^2 \mathbf{u} + \epsilon \mathbf{g}, \tag{A4}$$

where \mathbf{u} is the gas velocity, p is the gas pressure, ρ_g is the gas density, ν is the viscosity and ϵ is the local void fraction. Here, ϵ was determined from the positions of the particles using the ‘divided void fraction model’ implemented in *cfDEMcoupling*[®] (Kloss *et al.* 2012). The momentum exchange \mathbf{R} between the fluid and the particles inside a finite volume element ΔV was calculated as

$$\mathbf{R} = \frac{\sum_{j=1}^n \mathbf{F}_{d,j}}{\Delta V}. \tag{A5}$$

Here, the drag force $F_{d,j}$ was described by the Koch–Hill model (Koch & Hill 2001; van Buijtenen *et al.* 2011) as implemented in *cfDEMcoupling*[®] using the following relations:

$$\mathbf{F}_{d,j} = \frac{\pi}{6} d_j^3 \beta_j (\mathbf{u} - \mathbf{u}_{p,j}), \tag{A6}$$

$$\beta_j = \frac{18 \nu \rho_g \epsilon}{d_j^2} F, \tag{A7}$$

$$F = \epsilon \left(F_0 + \frac{1}{2} F_3 Re_p \right), \tag{A8}$$

$$F_0 = \begin{cases} \frac{1 + 3\sqrt{\frac{\epsilon_p}{2}} + \frac{135}{64} \epsilon_p \ln(\epsilon_p) + 16.14 \epsilon_p}{1 + 0.681 \epsilon_p - 8.48 \epsilon_p^2 + 8.16 \epsilon_p^3}, & \text{if } \epsilon_p < 0.4 \\ \frac{10 \epsilon_p}{\epsilon^3} & \text{if } \epsilon_p \geq 0.4 \end{cases}, \tag{A9}$$

$$F_3 = 0.0673 + 0.212 \epsilon_p + \frac{0.0232}{\epsilon^5}, \tag{A10}$$

with $\mathbf{u}_{p,j}$ the velocity of particle j . The local particle volume fraction ϵ_p was calculated as $1 = \epsilon_p + \epsilon$ and the particle-based Reynolds number Re_p is defined as $Re_p = d_j \epsilon |\mathbf{u} - \mathbf{u}_{p,j}| / \nu$.

Appendix B. Derivation of the gas shift model

The continuity equation of an incompressible gas flow of constant flow rate $Q = UW T$ that splits into two parallel flows is given by

$$Q/T = UW = (1 - W_c)u_b + W_c u_c. \quad (\text{B1})$$

Division by UW and introduction of $U_c^* = u_c/U$, $U_b^* = u_b/U$ and $W^* = W_c/W$ yields

$$1 = (1 - W^*)U_b^* + W^*U_c^*. \quad (\text{B2})$$

The pressure drop of a flow through a packing of height L is given by (Ergun 1952)

$$\frac{\Delta p_i}{L} = \frac{150\mu_g}{d_i^2} \frac{(1 - \epsilon_i)^2}{\epsilon_i^3} u_i + \frac{1.75\rho_g}{d_i} \frac{1 - \epsilon_i}{\epsilon_i^3} u_i^2, \quad (\text{B3})$$

where index $i = [b, c]$ denotes the bulk phase and the cluster phase (i.e. granular droplet/bubble), respectively, and $\mu_g = \nu\rho_g$ represents the dynamic gas viscosity. As $\Delta p_b/L = \Delta p_c/L$ and $\epsilon_b = \epsilon_c = \epsilon$, equating the pressure drop relations of the bulk and the cluster phase yields

$$0 = \left(u_b - \frac{u_c}{(d_c/d_b)^2} \right) + \frac{1.75d_b}{150(1 - \epsilon)\nu} \left(u_b^2 - \frac{u_c^2}{d_c/d_b} \right). \quad (\text{B4})$$

Now, we substitute $U_c^* = u_c/U$, $U_b^* = u_b/U$, $d^* = d_c/d_b$, $k = 150(1 - \epsilon)/1.75$ and $Re_b = Ud_b/\nu$ to form dimensionless groups giving

$$0 = \left(U_b^* - \frac{U_c^*}{d^{*2}} \right) + \frac{Re_b}{k} \left(U_b^{*2} - \frac{U_c^{*2}}{d^*} \right). \quad (\text{B5})$$

The combination of (B2) and (B5) determines the values of U_c^* and U_b^* for given d^* , W^* and Re_b .

Appendix C. Proof that $\Delta\rho^* = 1$ for $W^* \rightarrow 0$

The starting point of the neutral buoyancy limit for an infinitely small cluster ($W^* \rightarrow 0$) is the determination of the gas shift in/around the granular bubble/droplet. The continuity equation reads $U_b^* = 1$ and the pressure relation yields

$$0 = \left(1 - \frac{U_c^*}{d^{*2}} \right) + \frac{Re_b}{k} \left(1 - \frac{U_c^{*2}}{d^*} \right). \quad (\text{C1})$$

This expression is a quadratic equation that is solved for U_c^* with the positive solution

$$U_c^* = - (2k Re_b d^*)^{-1} + \sqrt{(2k Re_b d^*)^{-2} + d^* (k Re_b)^{-1} + d^*}. \quad (\text{C2})$$

Next, the minimum fluidization velocity of each particle type is determined by (Kunii & Levenspiel 1991)

$$\frac{1.75}{\epsilon^3} \left(\frac{d_i U_{mf,i}}{\nu} \right)^2 + \frac{150(1 - \epsilon)}{\epsilon^3} \left(\frac{d_i U_{mf,i}}{\nu} \right) = \frac{d_i^3 (\rho_i - \rho_g) g}{\rho_g \nu^2}, \quad (\text{C3})$$

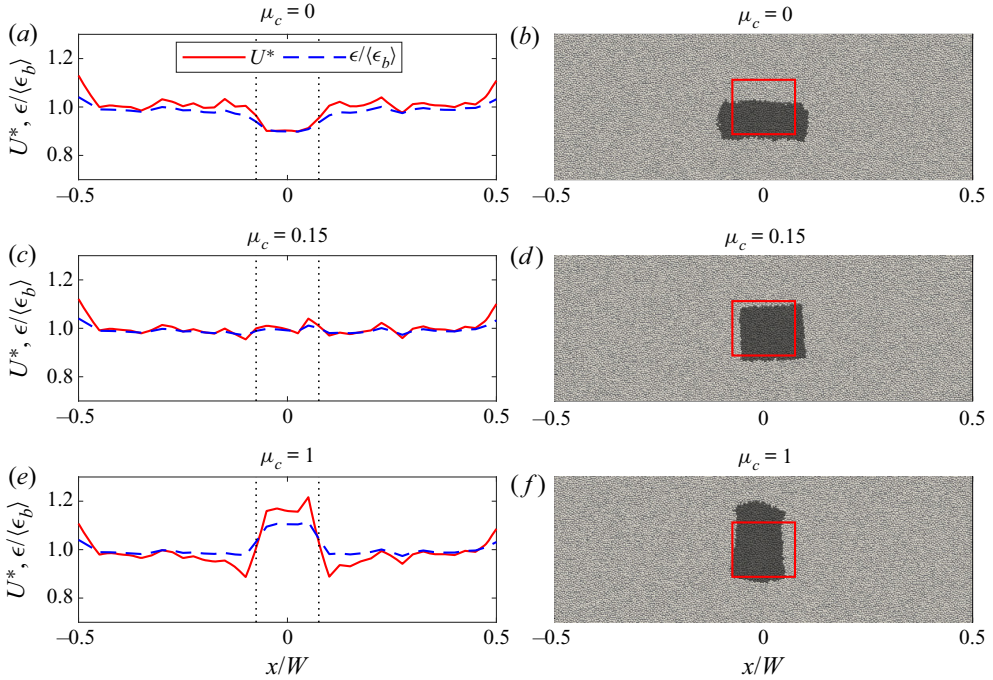


Figure 12. Influence of the coefficient of friction of the cluster particles μ_c on the evolution of a granular cluster with $d^* = 1$ and $\Delta\rho^* = 1$. Panels (a,c,e) show the value of U^* (red solid line) and $\epsilon/\langle\epsilon_b\rangle$ (blue dashed line) along a horizontal line through the centre of a granular cluster with $\mu_c = 0, 0.15$ and 1 , respectively. The black dotted lines represent the edges of the cluster at $|x/W| = W^*/2$. Panels (b,d,f) show the respectively forming granular clusters (dark grey), immersed in the bulk (light grey particles), after $t = 8$ s of vibro-gas-fluidization. The red rectangle marks the initial position of the granular cluster at $t = 0$ s. All results were obtained from simulations with $Re_b = 88.75$, $Ar_b = 3.4 \times 10^5$ and $\mu_b = 0.15$.

where we define $Ar_i = d_i^3(\rho_i - \rho_g)g/(\rho_g v^2)$, $Re_i = d_i U_{mf,i}/\nu$ and $i = [b, c]$, i.e.

$$\frac{1.75}{\epsilon^3} Re_i^2 + \frac{150(1 - \epsilon)}{\epsilon^3} Re_i = Ar_i. \tag{C4}$$

For $i = c$, this equation yields, by substituting $Re_c = Re_b d^* U_c^*$,

$$\frac{1.75}{\epsilon^3} Re_b^2 (d^* U_c^*)^2 + \frac{150(1 - \epsilon)}{\epsilon^3} Re_b d^* U_c^* = Ar_c. \tag{C5}$$

Next, the definition of k is inserted into (C2) and the result is then substituted into (C5). Simplifying the expression results in

$$d^{*3} \left[\frac{1.75}{\epsilon^3} Re_b^2 + \frac{150(1 - \epsilon)}{\epsilon^3} Re_b \right] = Ar_c. \tag{C6}$$

The bracketed term in (C6) can be replaced by Ar_b , yielding

$$d^{*3} Ar_b = Ar_c. \tag{C7}$$

Finally, re-substitution of the Ar_i definition and defining the relative density ratio to be

$$\Delta\rho^* = \frac{\rho_c - \rho_g}{\rho_b - \rho_g} \tag{C8}$$

On the rising and sinking of granular bubbles and droplets

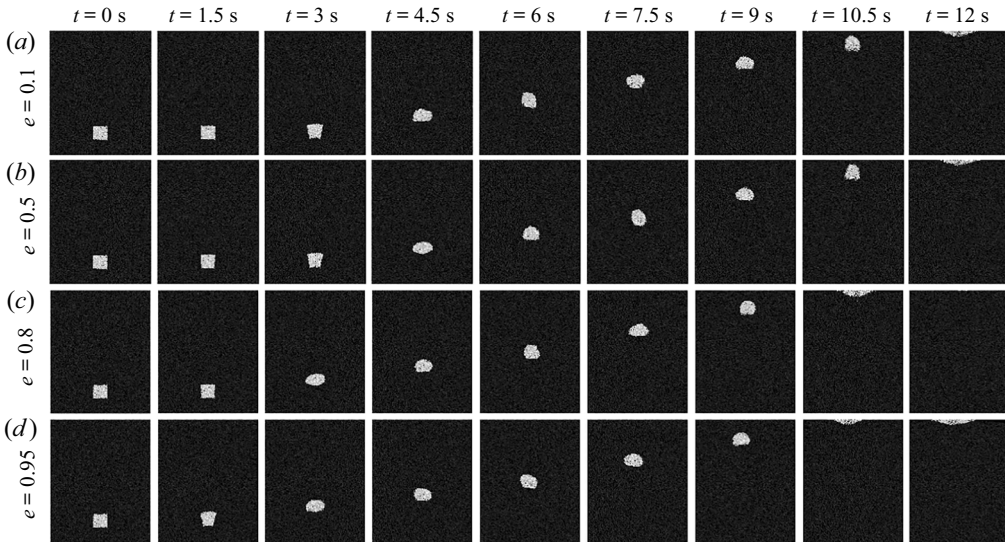


Figure 13. Effect of the coefficient of restitution e of the particles on the evolution of a granular bubble with $d^* = 1.5$ and $\Delta\rho^* = 0.417$. The coefficient of restitution increases from 0.1 (a) to 0.95 (d). Each column shows a snapshot of the granular bubble at the indicated time t after starting the vibro-gas-fluidization. Cluster particles are white, bulk particles are black. All results were obtained from simulations with $Re_b = 88.75$, $Ar_b = 3.4 \times 10^5$ and $\mu_b = 0.15$.

leads to

$$\rho_b - \rho_g = \rho_c - \rho_g \leftrightarrow \Delta\rho^* = 1. \quad (C9)$$

Appendix D. Effect of particle friction on the gas shift

Deriving (4.4), we assumed a constant local void fraction of $\epsilon \approx 0.4$ for both the granular cluster and its surrounding bulk. For spherical particles of comparable particle size distribution this is only fulfilled if the cluster particles and the bulk particles have similar coefficients of friction. Once the coefficient of friction of the cluster particles μ_c differs significantly from the coefficient of friction of the bulk particles μ_b , both particle types create packings of different void fraction. According to Ergun's equation (Ergun 1952), this leads to changes in the local permeability and influences the gas shift. To demonstrate the effect of void fraction on the dynamics of a granular cluster, additional simulation with $d^* = 1$ and $\Delta\rho^* = 1$ have been performed only changing the coefficient of friction of the cluster particles μ_c from 0 to 1 while μ_b was held constant at 0.15. This approach allowed us to initialize clusters of varying cluster void fraction ϵ_c . Except for the coefficient of friction, the cluster and bulk particles were identical. As can be seen in figure 12(e), the local void fraction ϵ_c in the cluster is higher than the average void fraction of the bulk phase $\langle\epsilon_b\rangle$, i.e. $\epsilon_c/\langle\epsilon_b\rangle = 1.15$, for $\mu_c = 1$. On the other hand, for $\mu_c = 0$, $\epsilon_c/\langle\epsilon_b\rangle = 0.91$, see figure 12(a). Due to these disturbances in the local void fraction, the fluidizing gas flows preferentially into the cluster ($U_c^* > 1$) for $\mu_c = 1$ and around the cluster ($U_c^* < 1$) for $\mu_c = 0$. As expected, for $\mu_c = 0.15$, no gas channelling occurs, see figure 12(c). The local increase/depletion of gas flow in the cluster leads to a condition in which the cluster particles are exposed to a gas velocity above/below $U_{mf,c}$ and thus rise/sink, respectively. Accordingly, the granular cluster stretches and rises for $\mu_c = 1$, flattens and sinks for $\mu_c = 0$, and does not deform significantly for $\mu_c = 0.15$, as can be seen in figure 12(b,d,f).

This finding supports our argument of neutral buoyancy for clusters that fulfil the condition $u_c = U_{mf,c}$. In addition, we see that the assumption of homogeneous void fraction is only fulfilled for beds containing particles of equal coefficients of friction. As the majority of our study was performed with $\mu_c = \mu_b = 0.15$, the effect of particle friction on the void fraction was neglected, justifying the simplification made in (4.4).

Appendix E. Effect of the coefficient of restitution on the motion of a granular bubble

Additional simulations have been performed to evaluate the effect of the coefficient of restitution e on the rise behaviour of a granular bubble. Varying e in a wide range from 0.1 to 0.95, we found only negligible influence of the value of e on the evolution of a granular bubble, as can be seen in figure 13. With increasing e , the rise of a granular bubble starts earlier, e.g. for $e = 0.95$ (d) the motion sets in before $t = 1.5$ s, whereas for $e = 0.1$ (a) no significant motion can be seen until $t = 3$ s. This is because the duration of the start-up phase until the entire bed is mobilized by vibration increases for decreasing e due to an increased rate of energy dissipation. However, the time required for the granular bubble to reach the top of the bed does not change significantly with e . Moreover, the shape of the rising bubble is hardly influenced by the value of e , as can be seen in figure 13. Thus, the use of a comparatively low value $e = 0.3$ to speed up the simulations is justifiable.

REFERENCES

- ALAM, M., TRUJILLO, L. & HERRMANN, H.J. 2006 Hydrodynamic theory for reverse Brazil nut segregation and the non-monotonic ascension dynamics. *J. Stat. Phys.* **124** (2), 587–623.
- BATCHELOR, G.K. 2000 *Flow of Effectively Inviscid Fluid with Vorticity*. Cambridge Mathematical Library, pp. 507–593. Cambridge University Press.
- BEESTRA, R., VAN DER HOEF, M.A. & KUIPERS, J.A.M. 2007 Numerical study of segregation using a new drag force correlation for polydisperse systems derived from Lattice–Boltzmann simulations. *Chem. Engng Sci.* **62** (1), 246–255, fluidized bed applications.
- BERZI, D. & FRACCAROLLO, L. 2015 Turbulence locality and granularlike fluid shear viscosity in collisional suspensions. *Phys. Rev. Lett.* **115**, 194501.
- BREU, A.P.J., ENSNER, H.M., KRUELLE, C.A. & REHBERG, I. 2003 Reversing the Brazil-nut effect: competition between percolation and condensation. *Phys. Rev. Lett.* **90**, 014302.
- VAN BUIJTENEN, M.S., VAN DIJK, W.-J., DEEN, N.G., KUIPERS, J.A.M., LEADBEATER, T. & PARKER, D.J. 2011 Numerical and experimental study on multiple-spout fluidized beds. *Chem. Engng. Sci.* **66** (11), 2368–2376.
- CARMAN, P.C. 1937 Fluid flow through granular beds. *Trans. Inst. Chem. Engrs* **15**, 150–166.
- CUNDALL, P.A. & STRACK, O.D.L. 1979 A discrete numerical model for granular assemblies. *Géotechnique* **29** (1), 47–65.
- DAVIDSON, J.F., HARRISON, D. & CARVALHO, J.R.F.G.D. 1977 On the liquidlike behavior of fluidized beds. *Annu. Rev. Fluid Mech.* **9** (1), 55–86.
- DURAN, J. 2001 Rayleigh–Taylor instabilities in thin films of tapped powder. *Phys. Rev. Lett.* **87** (25), 254301.
- ERGUN, S. 1952 Fluid flow through packed columns. *Chem. Engng Prog.* **48** (2), 89–94.
- GILBERTSON, M.A. & EAMES, I. 2001 Segregation patterns in gas-fluidized systems. *J. Fluid Mech.* **433**, 347–356.
- GOLDFARB, D.J., GLASSER, B.J. & SHINBROT, T. 2002 Shear instabilities in granular flows. *Nature* **415** (6869), 302–305.
- GUPTA, R. & MUJUMDAR, A.S. 1980 Aerodynamics of a vibrated fluid bed. *Can. J. Chem. Engng* **58** (3), 332–338.
- HADAMARD, J.S. 1911 Mouvement permanent lent d’une sphere liquide et visqueuse dans un liquide visqueux. *C. R. Hebd. Seances Acad. Sci.* **152**, 1735–1738.
- HILL, M.J.M. & HENRICI, O.M.F.E. 1894 VI. On a spherical vortex. *Phil. Trans. R. Soc. Lond.* **A 185**, 213–245.
- HONG, D.C., QUINN, P.V. & LUDING, S. 2001 Reverse Brazil nut problem: competition between percolation and condensation. *Phys. Rev. Lett.* **86** (15), 3423–3426.

On the rising and sinking of granular bubbles and droplets

- HUERTA, D.A. & RUIZ-SUÁREZ, J.C. 2004 Vibration-induced granular segregation: a phenomenon driven by three mechanisms. *Phys. Rev. Lett.* **92** (11), 114301.
- JENKINS, J.T. & YOON, D.K. 2002 Segregation in binary mixtures under gravity. *Phys. Rev. Lett.* **88**, 194301.
- KLOSS, C., GONIVA, C., HAGER, A., AMBERGER, S. & PIRKER, S. 2012 Models, algorithms and validation for opensource dem and CFD-DEM. *Prog. Comput. Fluid Dyn.* **12** (2–3), 140–152.
- KNIGHT, J.B., JAEGER, H.M. & NAGEL, S.R. 1993 Vibration-induced size separation in granular media: the convection connection. *Phys. Rev. Lett.* **70** (24), 3728–3731.
- KOCH, D.L. & HILL, R.J. 2001 Inertial effects in suspension and porous-media flows. *Annu. Rev. Fluid Mech.* **33**, 619–647.
- KOZENY, J. 1927 Über kapillare leitung des wassers im boden. *Royal Academy of Science Vienna, Proc. Class I* **136**, 271–306.
- KUNII, D. & LEVENSPIEL, O. 1991 *Chapter 3 – Fluidization and Mapping of Regimes*, pp. 61–94. Butterworth-Heinemann.
- LI, L., WU, P., REHMAN, A., WANG, L., ZHANG, S. & XIE, Z.-A. 2017a Energy-dissipation correlated size separation of granular matter under coupling vibration and airflow. *Powder Technol.* **307**, 84–89.
- LI, L., WU, P., ZHANG, S. & WANG, L. 2017b Diversity and controllability of particle distribution under coupling vibration and airflow. *Soft Matt.* **13** (39), 7034–7045.
- LI, L., WU, P., ZHANG, S. & WANG, L. 2019 Vertical separation criterion of binary particles under external excitation. *Powder Technol.* **342**, 404–408.
- LI, T., GOPALAKRISHNAN, P., GARG, R. & SHAHNAM, M. 2012 CFD-DEM study of effect of bed thickness for bubbling fluidized beds. *Particuology* **10** (5), 532–541.
- LI, T., ZHANG, Y. & HERNÁNDEZ-JIMÉNEZ, F. 2016 Investigation of particle-wall interaction in a pseudo-2D fluidized bed using CFD-DEM simulations. *Particuology* **25**, 10–22.
- LIU, C., WANG, L., WU, P. & JIA, M. 2010 Effects of gas flow on granular size separation. *Phys. Rev. Lett.* **104**, 188001.
- MAWATARI, Y., TATEMOTO, Y. & NODA, K. 2003 Prediction of minimum fluidization velocity for vibrated fluidized bed. *Powder Technol.* **131** (1), 66–70.
- MCLAREN, C.P., KOVAR, T.M., PENN, A., MÜLLER, C.R. & BOYCE, C.M. 2019 Gravitational instabilities in binary granular materials. *Proc. Natl Acad. Sci. USA* **116** (19), 9263–9268.
- MCLAREN, C.P., METZGER, J.P., BOYCE, C.M. & MÜLLER, C.R. 2021 Reduction in minimum fluidization velocity and minimum bubbling velocity in gas-solid fluidized beds due to vibration. *Powder Technol.* **382**, 566–572.
- METZGER, J.P., MCLAREN, C.P., PINZELLO, S., CONZELMANN, N.A., BOYCE, C.M. & MÜLLER, C.R. 2022 Sinking dynamics and splitting of a granular droplet. *Phys. Rev. Fluids* **7**, 014309.
- NITSCHKE, J.M. & BATCHELOR, G.K. 1997 Break-up of a falling drop containing dispersed particles. *J. Fluid Mech.* **340**, 161–175.
- PUSEY, P.N. 1987 The effect of polydispersity on the crystallization of hard spherical colloids. *J. Phys.* **48** (5), 709–712.
- ROSATO, A., STRANDBURG, K.J., PRINZ, F. & SWENDSEN, R.H. 1987 Why the Brazil nuts are on top: size segregation of particulate matter by shaking. *Phys. Rev. Lett.* **58** (10), 1038–1040.
- RYBCZYNSKI, W. 1911 Über die fortschreitende bewegung einer flüssigen kugel in einem zähen medium. *Bull. Acad. Sci. Cracovie A* **1**, 40–46.
- SHINBROT, T. 2004 Granular materials - the Brazil nut effect - in reverse. *Nature* **429** (6990), 352–353.
- SOMMERFELD, M. 2018 *Bewegung fester Partikel in Gasen und Flüssigkeiten*, pp. 1–17. Springer.
- TRUJILLO, L., ALAM, M. & HERRMANN, H.J. 2003 Segregation in a fluidized binary granular mixture: competition between buoyancy and geometric forces. *Europhys. Lett.* **64** (2), 190–196.
- TSUJI, Y., KAWAGUCHI, T. & TANAKA, T. 1993 Discrete particle simulation of two-dimensional fluidized bed. *Powder Technol.* **77** (1), 79–87.
- VINNINGLAND, J.L., JOHNSEN, Ø., FLEKKØY, E.G., TOUSSAINT, R. & MÅLØY, K.J. 2007 Granular Rayleigh-Taylor instability: experiments and simulations. *Phys. Rev. Lett.* **99**, 048001.
- ZENIT, R., HUNT, M.L. & BRENNEN, C.E. 1997 Collisional particle pressure measurements in solid-liquid flows. *J. Fluid Mech.* **353**, 261–283.
- ZHOU, Z.Y., KUANG, S.B., CHU, K.W. & YU, A.B. 2010 Discrete particle simulation of particle-fluid flow: model formulations and their applicability. *J. Fluid Mech.* **661**, 482–510.